Numerical-modeling-based investigation of sound transmission and reception in the short-finned pilot whale (*Globicephala macrorhynchus*)

Zhongchang Song, Jinhu Zhang, Wenzhan Ou, et al.

Citation: The Journal of the Acoustical Society of America **150**, 225 (2021); doi: 10.1121/10.0005518
View online: https://doi.org/10.1121/10.0005518
View Table of Contents: https://asa.scitation.org/toc/jas/150/1
Published by the Acoustical Society of America

JASA ARTICLE

Numerical-modeling-based investigation of sound transmission and reception in the short-finned pilot whale (*Globicephala macrorhynchus*)

Zhongchang Song,[1,a)] Jinhu Zhang,[2] Wenzhan Ou,[2] Chuang Zhang,[2] Lijun Dong,[3] Jianchen Dong,[3] Songhai Li,[3,b)] and Yu Zhang[2,c)]

[1]*State Key Laboratory of Marine Environmental Science, College of the Environment and Ecology, Xiamen University, Xiamen 361005, Fujian, China*

[2]*Key Laboratory of Underwater Acoustic Communication and Marine Information Technology of the Ministry of Education, College of Ocean and Earth Sciences, Xiamen University, Xiamen 361005, Fujian, China*

[3]*Marine Mammal and Marine Bioacoustics Laboratory, Institute of Deep-sea Science and Engineering, Chinese Academy of Sciences, Sanya 572000, China*

ABSTRACT:

The sound-transmission, beam-formation, and sound-reception processes of a short-finned pilot whale (*Globicephala macrorhynchus*) were investigated using computed tomography (CT) scanning and numerical simulation. The results showed that sound propagations in the forehead were modulated by the upper jaw, air components, and soft tissues, which attributed to the beam formation in the external acoustic field. These structures owned different acoustic impedance and formed a multiphasic sound transmission system that can modulate sounds into a beam. The reception pathways composed of the solid mandible and acoustic fats in the lower head conducted sounds into the tympano-periotic complex. In the simulations, sounds were emitted in the forehead transmission system and propagated into water to interrogate a steel cylinder. The resulting echoes can be interpreted from multiple perspectives, including amplitude, waveform, and spectrum, to obtain the acoustic cues of the steel cylinder. By taking the short-finned pilot whale as an example, this study provides meaningful information to further deepen our understanding of biosonar system operations, and may expand sound-reception theory in odontocetes.

 https://doi.org/10.1121/10.0005518

(Received 24 March 2021; revised 9 June 2021; accepted 14 June 2021; published online 12 July 2021)

[Editor: Klaus Lucke] Pages: 225–232

I. INTRODUCTION

Odontocetes of all sizes can use ultrasound to detect and prey upon targets (Au, 1993; Cranford *et al.*, 1996). Their ability to echolocate was first demonstrated over six decades ago (Schevill and Lawrence, 1956; Kellogg, 1958; Norris *et al.*, 1961) and has been further confirmed in various experiments. Odontocetes whose eyes are covered can still avoid obstacles and complete challenging tasks by emitting ultrasound (Norris *et al.*, 1961; Busnel and Dziedzic, 1967). The subsequent decades have witnessed the development of bio-sonar research in odontocetes. In 1996, Cranford *et al.*, used computed tomography (CT) scanning to investigate the nasal complex of 40 samples, and they proposed a standard mechanism for sound generation in odontocetes (Cranford *et al.*, 1996): Odontocetes generate ultrasounds using their dorsal bursae and monkey lips, which form a complex that is forced to vibrate under pressurized air from the nares; adjacent air sacs facilitate the recycling of air and generate a periodically repeating sound (Cranford *et al.*, 1996).

After generation, sounds are transmitted to the forehead, which contains fat, muscles, and connective tissues (Aroyan *et al.*, 1992; Cranford *et al.*, 2008; Song *et al.*, 2015). These soft tissues have different acoustic impedances, which produce a gradient distribution from inner core to outer layers in forehead. The sounds are modulated by the interactions between soft tissues, solid skull structures, and air sacs, thereby forming sound beams (Aroyan *et al.*, 1992). The solid upper jaw functions as a seat base for soft tissues and can induce interfacial waves along the solid–fluid interface (Song *et al.*, 2016). Wisniewska *et al.* (2015) determined that the harbor porpoise can adjust its sound beam (acoustic window) when approaching targets. This adjustment may help in target discrimination, which has been considered from multiple perspectives, including investigation of the materials, shapes, and wall thicknesses of targets (Evans and Powell, 1967; Au and Turl, 1991; Aubauer *et al.*, 2000; Au *et al.*, 1980; Pack *et al.*, 2002; Au and Pawloski, 1992). Odontocetes possess a sophisticated biosonar system to distinguish targets based on echo features in both the time and frequency domains and can efficiently fulfill target detection in a long range (Madsen *et al.*, 2004; Au

[a)]Also at: Biology Department, Woods Hole Oceanographic Institution, Woods Hole, MA 02543, USA, ORCID: 0000-0002-5259-5718.
[b)]ORCID: 0000-0003-4977-1722.
[c)]Electronic mail: yuzhang@xmu.edu.cn, ORCID: 0000-0001-6183-0612.

et al., 2007; Au *et al.*, 2009). Considerable knowledge has been obtained regarding the target-detection operations of odontocetes' bio-sonar systems. However, in most studies, the echoes expressing acoustic features of the targets were received by receptors located in water. No studies have sought to analyze odontocetes' echo-reception systems because it is unethical to implant sensors into live animals. The problem can be approached via numerical modeling (Cranford *et al.*, 2008; Song *et al.*, 2018).

Sounds can reach the odontocetes' ear complex via various pathways (Norris 1964, 1968; Cranford *et al.*, 2008; Song *et al.*, 2018; Popov *et al.*, 2019). The external mandibular fat located between the skin and a thin portion of the posterior mandible known as the "pan-bone" constitutes an important sound entrance. Upon entry, sounds traverse the pan-bone, reach the internal mandibular fat, and are then conducted further into the ear complex. This "jaw hearing" pathway proposed by Norris has been confirmed by subsequent experiments (Bullock *et al.*, 1968; Brill *et al.*, 1988; Brill and Harder, 1991; Møhl *et al.*, 1999). Using finite element modeling, Cranford *et al.* (2008) identified an additional sound-reception pathway—the so-called "gular pathway"—by which sounds enter the internal mandibular fat through the ventral margin of the mandible; these findings were based on a case study of a Cuvier's beaked whale (*Ziphius cavirostris*). In addition, sound-reception channels in which the solid mandible may play a significant role were introduced in both the experiments and numerical models (Castellote *et al.*, 2014; Mooney *et al.*, 2008; Mooney *et al.*, 2015; Mooney *et al.*, 2018; Song *et al.*, 2018). These results indicate that the entire head may function as an antenna system for sound reception (Popov *et al.*, 2019).

Odontocetes echolocation involves sound-generation, transmission, beam-formation, and sound-reception processes (Au, 1993; Cranford *et al.*, 1996; Norris, 1964, 1968). In this study, we used the short-finned pilot whale (*Globicephala macrorhynchus*) as an example, investigating these processes. Short-finned pilot whale populations are distributed around the globe in warm temperate zones, and they inhabit offshore waters (Olsen, 2009). This species has an almost negligible beak and bulbous melon. The sound speed and density of soft tissues in its bio-sonar transmission system are within the ranges 1224–1749 m/s and 874–1090 kg/m^3, respectively (Dong *et al.*, 2017). This species emits echolocation clicks, which predominately peak below 40 kHz (Baumann-Pickering *et al.*, 2015); meanwhile, they can hear up to high frequencies over 100 kHz, with a peak sensitivity in the range 20–40 kHz (Greenhow *et al.*, 2014). Much work remains to be performed regarding the echolocation capacities of this species' bio-sonar system. We combined CT and numerical simulations to enhance our understanding of these whales' echolocation process.

II. MATERIAL AND METHODS

In 2016, a female short-finned pilot whale was found dead in Lingshui waters, Hainan Province, China; it was immediately frozen at −20 °C. The whale was considered to be freshly dead, because no obvious decomposition was noted (Dong *et al.*, 2017). After 20 days, the specimen was removed to be naturally thawed. The head was cut such that it could be scanned in a CT machine. The forehead soft tissue pack was extracted and cut into small pieces for sound speed and density measurements. More details can be found in our previous study (Dong *et al.*, 2017). Here, a brief introduction to the model development is provided. The sound emission and reception systems are located at the forehead and lower head, respectively (Fig. 1). We

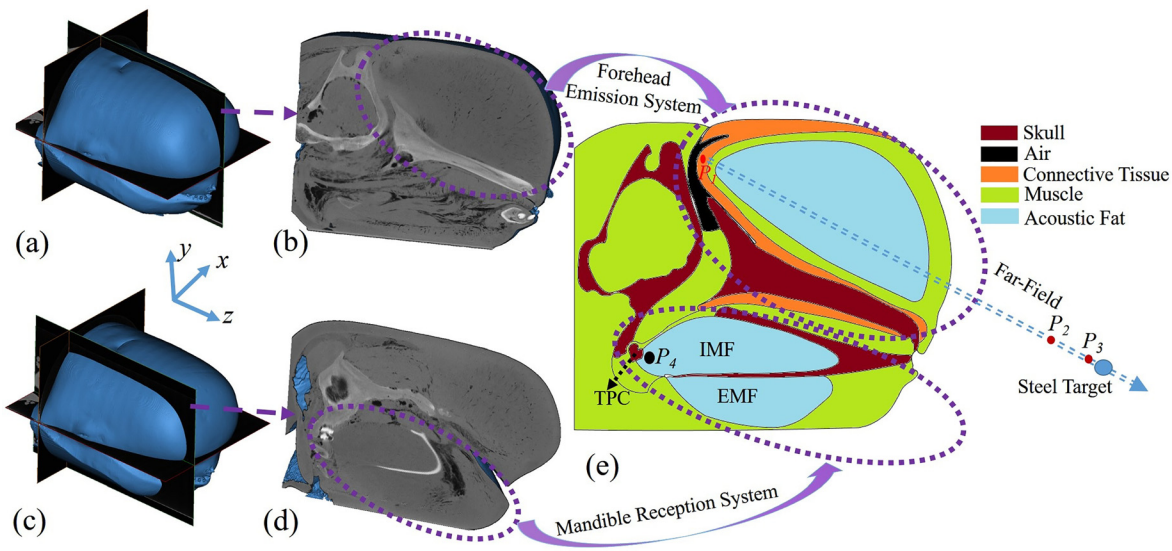

FIG. 1. (Color online) (a) The reconstructed sound-transmission system of the short-finned pilot whale, represented in three dimensions. (b) Projected transmission plane. (c) Reconstructed sound-reception system. (d) Projected sound-reception plane. (e) Geometrical model depicting the integrity of the sound-transmission and -reception systems. The major components of the bio-sonar transmission and reception systems are the skull, air, acoustic fats, muscle, and connective tissue. IMF: internal mandibular fat; EMF: external mandibular fat; P_1: sound source; P_2: reception point in far field; P_3: reception point near the steel target; P_4: reception point in sound reception pathway near the tympano-periotic complex (TPC).

https://doi.org/10.1121/10.0005518

combined these two systems to construct a complete SONAR model [Fig. 1(e)].

A model of the emission system pathway in the sagittal plane (y-z plane), located slightly to the right of the blowhole, was developed [Fig. 1(e)] by referring to the obtained anatomy [Figs. 1(a) and 1(b)]. The sagittal plane of the reception system was also reconstructed, to provide geometrical information for the subsequent model-development stages [Figs. 1(c) and 1(d)]. The appropriate sound speeds and densities of the transmission [Fig. 2(a)] and reception [Figs. 2(b) and 2(c)] systems were assigned in the numerical model. Alongside soft tissues, the model contained skull and air components, whose compressional sound-wave speeds and densities were set as 3380 m/s and 2035 kg/m^3, and 343 m/s and 1.12 kg/m^3(Graf *et al.*, 2008; Song *et al.*, 2016). The shear wave speed of the solid skull structures was set to 2200 m/s. The integrated model was placed in a circular water environment of radius 1.5 m, and the sound speed and density of water were set as 1500 m/s and 998 kg/m^3, respectively.

COMSOL Multiphysics software (Stockholm, Sweden) was used to compute the wave propagation and beam formation in finite elements. The computational domain was meshed with 10 elements per wavelength. Acoustic theories describing sound-wave propagation in fluid and solid media have been proposed (Aroyan *et al.*, 1992; Song *et al.*, 2016). First, we examined the wave propagation through the transmission system and the formation of the main beam and side lobes in the time domain. A short-duration pulse was triggered at the sound source [point P_1 in Fig. 1(e)] as follows:

$$Q_m = A_0 e^{(\alpha_1 t + \alpha_2 t_1)} \sin 2\pi f_0 t \quad 0 \le t \le t_1, \tag{1}$$

$$Q_m = A_1 e^{(-\alpha_1 t + \alpha_1 t_2)} \sin 2\pi f_0 t \quad t_1 \le t \le t_2, \tag{2}$$

where A_0 and A_1 are the parameters to set relative amplitudes and f_0 is the peak frequency, which was set to 20 kHz (Baumann-Pickering *et al.*, 2015). α_1 and α_2 are parameters used to control the pulse bandwidth; t_1 and t_2 quantitatively control the times of signal onset, peak location, and closure; and t is the time variable. The resulting waveform and spectrum of the source pulse were shown in Fig. 3. These parameters were based on a previous report of clicks for this species (Baumann-Pickering *et al.*, 2015). Next, the simulation was extended to target detection and sound reception. A circular target model (radius: 0.04 m) of steel was positioned 1 m away from the sound source. The speeds of the compressional and shear waves were set as 6144 and 3095 m/s for the steel and density was set as 7850 kg/m^3 (Feng *et al.*, 2019). The echo propagation was examined in detail, to identify the various pathways through which sounds are conducted to the tympano-periotic complex (TPC). The sound pulse was activated at the sound source, and the sound waves propagated through the forehead into water. After reaching the target, the backward-reflected waves (echoes) containing acoustic features of the target were propagated toward the model of the head; these were tracked at reception points P_3 near the target and P_4 near the tympano-periotic complex (TPC). Finally, the waveforms and amplitudes of echoes received at these two locations were compared to examine the modulation of sound reception pathway on echoes.

III. RESULTS

Six propagation snapshots were obtained in succession (Fig. 3), indicating that sounds mostly propagated forward, parallel to the upper jaw extension, producing a main beam

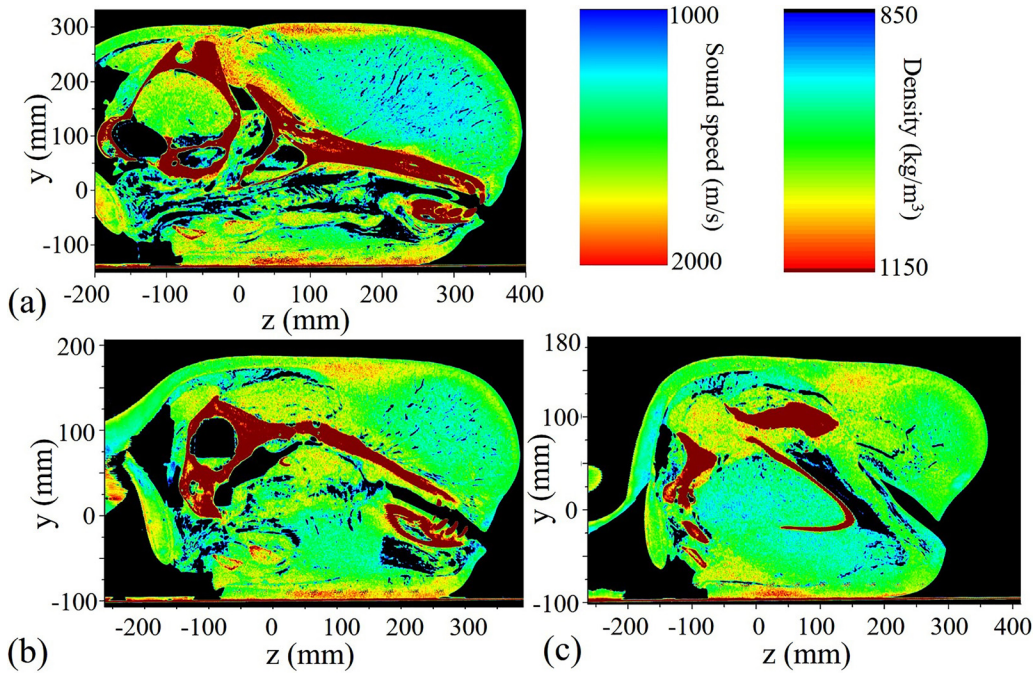

FIG. 2. (Color online) Sound speed and density reconstructions of the short-finned pilot whale's sound-transmission and -reception systems in the sagittal (y-z) plane: (a) transmission system, (b) plane 1, and (c) plane 2 of the sound-reception system.

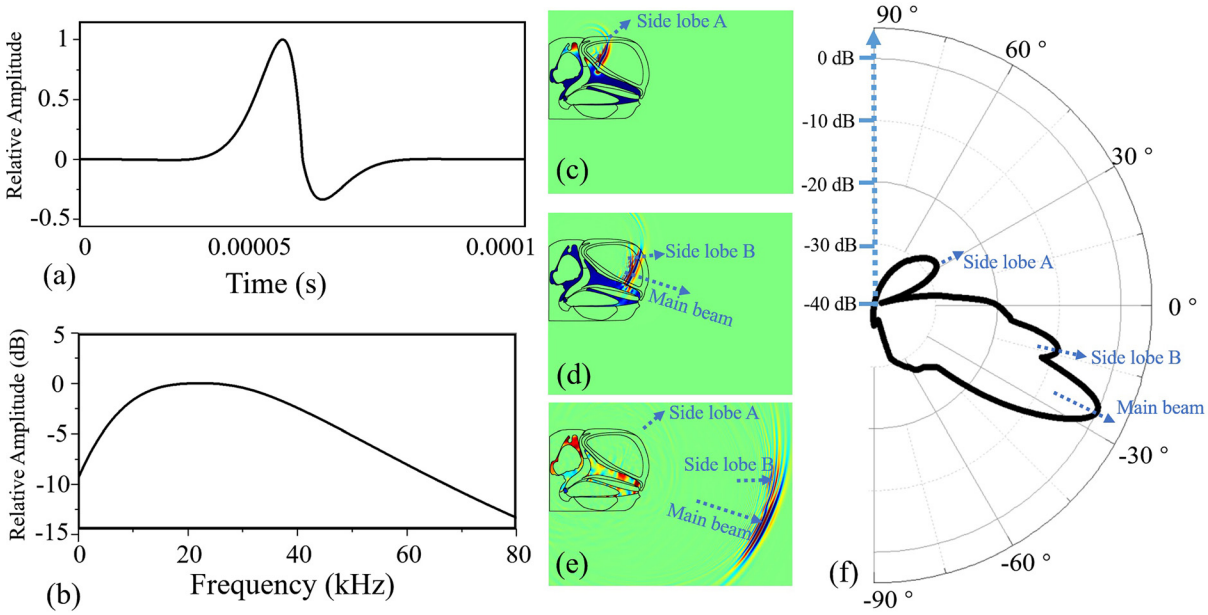

FIG. 3. (Color online) Sound excitation in the (a) time domain and (b) frequency domain. Propagation plots for the transient sound waves at (c) 150 μs, (d) 300 μs, and (e) 800 μs. (f) Beam pattern. The formation of the main and side beams was determined by initial wave propagations within the forehead sound-transmission system.

with a –3 dB bandwidth of 8.2° [Figs. 3(e) and 3(f)]. A fraction of the sound waves was reflected by the media interfaces, producing side lobes. The main-beam and sidelobe characteristics in the external field were attributed to wave propagation in the internal forehead transmission system, which was controlled by the interaction of forehead soft tissues, solid skull structures, and air spaces. Aside from acting as a reflector, the solid upper jaw also functioned as an interfacial wave conductor [Figs. 3(c) and 3(d)], inducing a series of waves that merged with those generated by the soft tissues at the upper jaw tip to propagate further into the water. The main beam was oriented almost −30° downward, in contrast to the upward angle obtained for bottlenose dolphins (Au *et al.*, 1978; Au, 1993). The short-finned pilot whale has a longer and more skewed downward upper jaw than the bottlenose dolphin. This may produce different main-beam orientations between the two species, because the upper jaw is an important sound reflector that can influence the beam formation (Aroyan *et al.*, 1992). These details suggest a complex physical mechanism in the beam-formation process of the short-finned pilot whale.

The sound-transmission complexity was also reflected in the differences between the near and far fields [Fig. 4(a)]. We distributed individual reception points along the main beam axis between the sound source P_1 (0, 0) and furthest point (1.2 m, 0), with an interval of 0.05 m along the z axis. The waveform of the signal at point P_2 is provided as an example. The amplitude of the received signal at these points was tracked, and a dynamic trend was observed [Fig. 4(a)]. The entire computational domain was roughly divided into three subfields [Fig. 4(b) and 4(c)]: internal head field (*R1*), near field (*R2*), and far field (*R3*). In the internal head field, the pressure amplitude fluctuated dramatically and entered the far field rapidly (below 0.1 m) after the sound left the head. Thereafter, the signal amplitude decreased monotonically with distance.

In our simulations, we placed a steel target model within the main beam window in the far field region. Echoes from the target reached the anterior head; then, a series of sound waves were induced to propagate along the mandible and through the internal mandibular fat [Figs. 5(b) and 5(c)]. Another series traveled along the external mandibular fat and was further redirected towards the ear complex [Figs. 5(c) and 5(d)]; this is consistent with the "jaw-hearing pathway" and "gular pathway" proposed by Norris (1964, 1968) and Cranford *et al.* (2008), respectively. The main peak of the echoes near the target was followed by reflection signals from the steel; this produced many narrow peaks in the spectrum, as noted in other studies (Au and Pawloski, 1992; Qiao *et al.*, 2017; Feng *et al.*, 2019). More importantly, in this study, we found that after propagating along the sound-reception pathway, the echoes changed in both the time and frequency domains. Although the relative energy amplitude distribution remained almost unchanged in the low-frequency range for echoes received at P_3 and P_4, a slight frequency shift was indicated in the spectrum peaks between these two cases, and considerable energy attenuation was observed above 100 kHz [Fig. 5(h)] compared to the example in Fig. 5(f).

The sound propagation inside the head suggested that the mandible and internal fat formed an important pathway (pathway 1 in Fig. 6), guiding a certain proportion of the sounds into the TPC (Fig. 6). After sounds originating from the front of the head model made contacted with the lower region [Fig. 6(a)], waves were induced in the mandible and

https://doi.org/10.1121/10.0005518

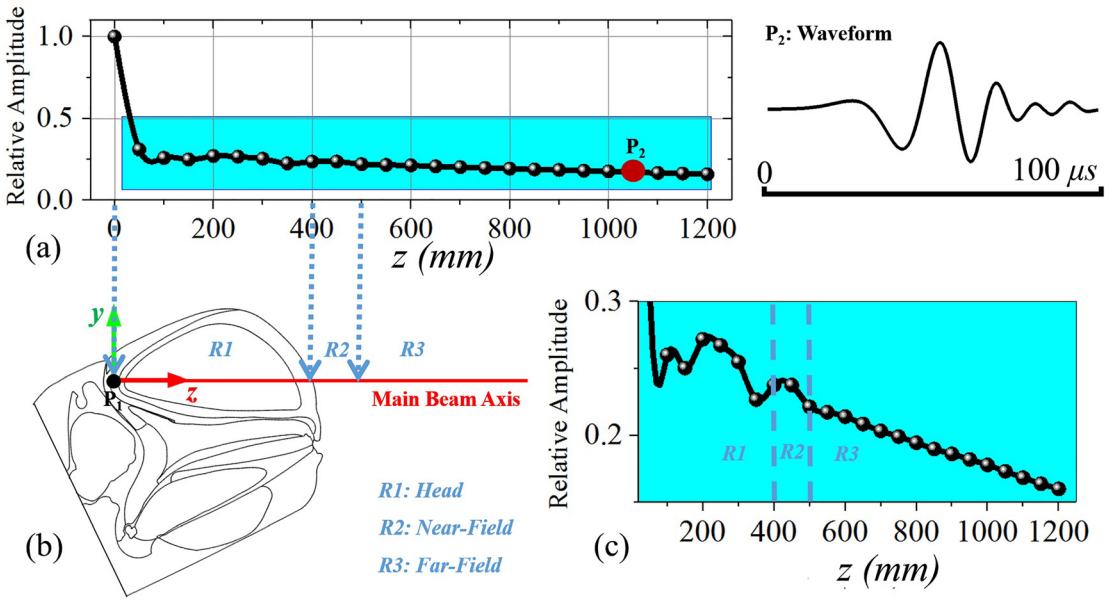

FIG. 4. (Color online) (a) Amplitude distribution of signals received at distinct points along the main beam axis; here, the signal waveform of point P_2 is given as an example. (b) Acoustic field sections along main beam axis. (c) Amplitude distribution of signals separated over an expanded range.

propagated to the pellucid fat located within its internal cavity [Figs. 6(c) and 6(h)]. These waves were then propagated posteriorly along the internal mandible and merged with those from another pathway (pathway 2) before finally arriving at the TPC. In pathway 2, the external mandibular fat played a primary role in transferring sounds to the TPC. The series of sound waves propagated along pathway 2 are depicted by arrows in Figs. 6(g), 6(h), and 6(i). Sounds entered the internal mandibular fat channel via the posterior mandible and external mandibular fats before reaching the TPC; this is similar to the pathways described in the jaw hearing and "gular" pathway theories (Norris *et al.*, 1961; Norris, 1964, 1968; Cranford *et al.*, 2008). The sounds from these different pathways were aggregated as the final acoustic stimuli for the TPC.

IV. DISCUSSION AND CONCLUSIONS

A. Sound transmission and reception

The sound-transmission and -reception pathways were not located in the same sagittal plane. In previous two-dimensional models, these two systems were typically separated into their respective models (Zhang *et al.*, 2017; Song *et al.*, 2018). However, this restricts our understanding of

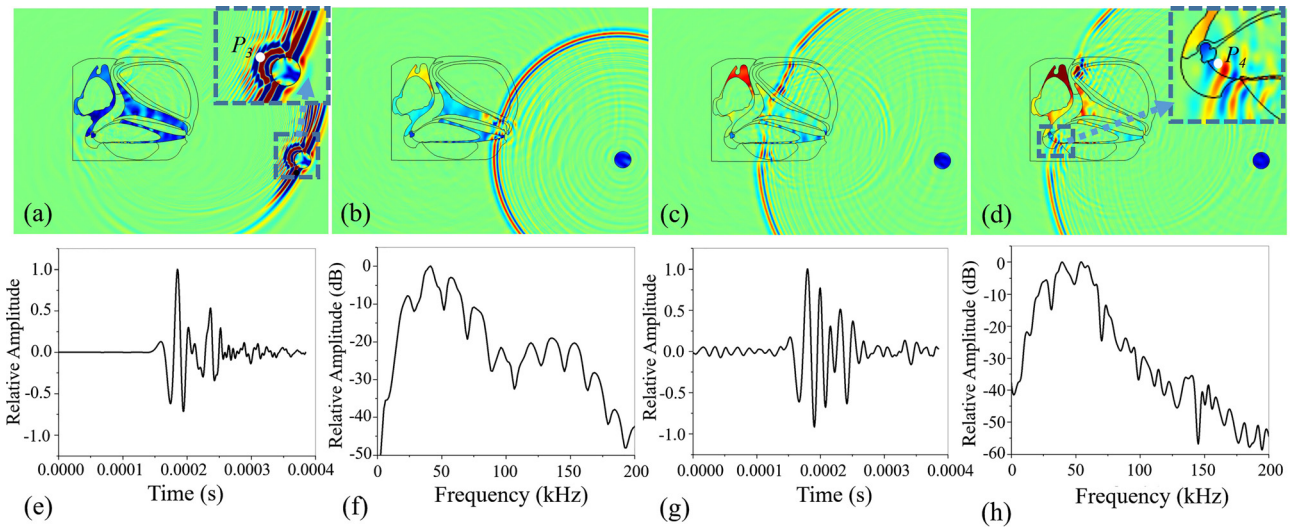

FIG. 5. (Color online) (a) Propagation of echoes from steel at t_1, where a reception point P_3 was set near the steel to track echoes. (b) Propagation of echoes at t_2, where waves were partially induced to propagate along the mandible. (c) Propagation of echoes at t_3, where waves were observed to propagate along the external and internal mandibular fats. (d) Propagation of echoes at t_4, where the reception point P4 was set in the sound-reception pathway near the tympano-periotic complex (TPC). (e) Time series of echoes at point P_3. (f) Spectrum of echoes at point P_3. (g) Time series of echoes at point P_4. (h) Spectrum of echoes at point P_4.

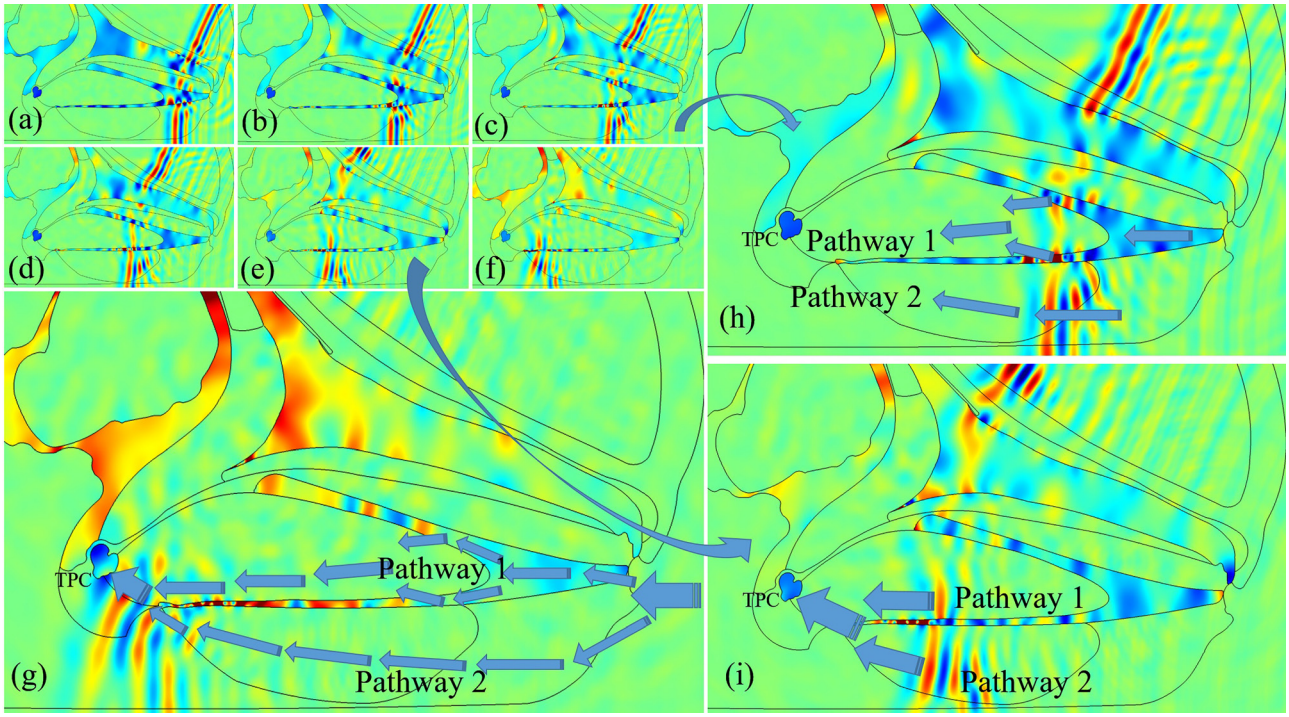

FIG. 6. (Color online) Propagation of target echoes along the reception pathways of the short-finned pilot whale at (a) t_1, (b) t_2, (c) t_3, (d) t_4, (e) t_5, (f) t_6, and (g) t_7; meanwhile, (h) and (i) depict the enlarged propagation details at times t_3 and t_5. The sound waves were propagated to the TPC by two separate series. In pathway 1, the wave series was first propagated along the mandible to reach the internal mandibular fat. In pathway 2, sound waves travelled along the external mandibular fat and traversed the mandible to reach the internal mandibular fat. The sound waves from these two pathways merged before finally arriving at the TPC.

the bio-sonar target-detection capabilities. Using a full echolocation model, we can deepen our understanding of the beam properties and sound reception mechanisms of short-finned pilot whales. The radiating acoustic field entered the far field within a short distance (0.5 m) of the source, similar to the results obtained for bottlenose dolphins (Au *et al.*, 1978; Finneran *et al.*, 2016). Short-finned pilot whales have a larger head than finless porpoises and harbor porpoises. The –3 dB beam width was 8.2° for the short-finned pilot whale, smaller than the values of 16.5° (*Phocoena phocoena*, Au *et al.*, 1999) and 13.3° (*N. a. sunameri*, Zhang *et al.*, 2017) and comparable to the values of 9.7° (*Pseudorca crassidens*, Au *et al.*, 1995) and 6.5° (*Delphinapterus leucas*, Au, 1993) obtained for other species with obtuse heads as well. The acoustic field and beam properties can be influenced by factors such as the frequency of bio-sonar clicks and size and shape of head (Au *et al.*, 1999; Urick, 1983). More samples are necessary to determine whether this inversely proportional relationship between head size and beam width is more widely applicable in odontocetes (Au *et al.*, 1999).

Odontocetes can generate sounds to form beams. Air-filled structures (e.g., the air sac and nasal passage) can prevent the sound energy from leaking backward and upward, focusing the majority of sound energy into the forward direction. These conclusions regarding the roles of acoustic structures in sound-beam formation are consistent with those of previous studies (Aroyan *et al.*, 1992; Zhang *et al.*, 2017; Wei *et al.*, 2017). Acoustic fats exhibit the lowest sound speeds and densities of soft tissues, and they are important waveguides in both the sound-transmission and -reception processes. Echoes can stimulate waves to travel along the mandible, posteriorly to the internal mandibular fat; these waves eventually arrive at the TPC. This bone-tissue sound-reception pathway, identified in the finless porpoise (*N. a. sunameri*), proves reliable in short-finned pilot whales as well. The sound-reception process is complicated, embodied in various pathways, and includes the "jaw hearing," "gular," and mandible–mandibular fat pathways (Norris, 1964; Cranford *et al.*, 2008; Song *et al.*, 2018).

In the present study, when sounds entered the front portion of the lower head, the anterior mandible and soft tissues acted as the entrances of the two respective pathways. The sounds from these two pathways were finally aggregated before reaching the TPC. We have previously examined similar sound pathways for finless porpoises (*N. a. sunameri*), in which higher-peak-frequency (exceeding 100 kHz) clicks (Song *et al.*, 2018) were used. Using a relatively lower-peak-frequency (20 kHz) sound pulse in the current simulations, we showed that the mandible-mandibular pathway is also reliable for lower-frequency acoustic stimuli, though in a different species. The TPC is accessible to sounds propagating through various pathways, and the entire head may function as a volume antenna to conduct sounds as acoustic cues for hearing (Popov *et al.*, 2019). Further studies are needed to quantify the respective contributions of these pathways in hearing. These pathways may influence the directivity of hearing in odontocetes, many species of

which exhibit a variable sensitivity to sounds approaching from different directions (Au and Moore, 1984; Møhl *et al.*, 1999; Aroyan, 2001).

B. Comparison of echoes at different locations

Numerous odontocetes can effectively use the spectral and temporal cues of echoes as well as combinations thereof to discriminate different targets (Nachtigall, 1980; Delong *et al.*, 2006). Such cues include target strength, number of highlights in the echo waveform, and spectral contours (Au and Pawloski, 1992). These reflect the physical features (size, shape, material, and thickness) of the targets and are informative for discrimination (Au and Pawloski, 1992; Au *et al.*, 1980; Au *et al.*, 2009).

To quantitatively describe the physical characteristics expressed via echoes, previous studies have used biomimetic clicks emitted by a transducer to interrogate targets; the echoes were then used for further analysis of fish discrimination (Au *et al.*, 2007; Au *et al.*, 2009). These studies made available numerous research options for studying the target-detection capabilities of odontocetes' bio-sonar systems; however, the target echoes were recorded in the water, instead of the internal sound-reception system (Feng *et al.*, 2019). Implanting recording equipment inside animals is unethical, because of the destructive effects it entails. Hence, numerical modeling is an important complement to experiments, helping to investigate the physical mechanisms of bio-sonar systems in odontocetes (Aroyan *et al.*, 1992; Cranford *et al.*, 2008).

Inspired by previous numerical studies (Cranford *et al.*, 2008; Song *et al.*, 2018), we extracted echoes from the internal sound-reception pathways of short-finned pilot whales. The echoes received at different reception points exhibited clear variations in their waveforms and spectral distributions (Fig. 5). The spectral characteristics of the echoes [Figs. 5(f) and 5(h)] received at reception points P_3 [Fig. 5(a)] and P_4 indicate that, in the frequency range 100–150 kHz, greater energy attenuation occurred along the sound-reception pathway [Fig. 5(h)]. This suggests the potential modulation effect of the sound-reception pathway on the echoes. In future studies (especially modeling-based ones), echoes should be examined inside the sound-reception pathway, rather than at locations near the targets. Odontocetes exhibit a consistently good sensitivity to high-frequency sounds, but within a certain range. When the frequency of acoustic stimuli extends further to over 128 kHz, the sensitivity usually becomes poor (Castellote *et al.*, 2014; Mooney *et al.*, 2018; Li *et al.*, 2012). Therefore, we deem it worthwhile to investigate the potential relationship between the hearing sensitivity and modulation of sound-reception pathways in future studies.

Much work remains to be performed on sound-emission, reception, and target-detection in odontocetes. Our modeling results suggest that sound-reception pathways can modulate the echoes and weaken the relative sound energies at high frequencies. These results can contribute to the understanding of the sound-transmission and -reception pathways in short-finned pilot whales. The acoustic cues of target echoes are fundamental in discrimination. Furthermore, the sound-reception process is important and should be considered in future studies when odontocete bio-sonar models are used to obtain echoes. The approach constructed in this study can be applied to other species, particularly those implementing models to investigate target detection.

ACKNOWLEDGMENTS

This work was financially supported by the project supported by the National Key Research and Development Program of China (Grant Nos. 2018YFC1407505, 2018YFC1407504, 2016YFC0300802, and 2018YFC0308602), the National Natural Science Foundation of China (Grant Nos. 12074323 and 41422604), the Special Fund for Marine and Fishery Development of Xiamen (Grant No. 20CZB015HJ01), Water Conservancy Science and Technology Innovation Project of Guangdong (Grant No. 2020-16), the China Postdoctoral Science Foundation (Grant No. 2020M682086), and the China National Postdoctoral Program for Innovative Talents (Grant No. BX2021168). We are grateful to Xiaohui Xu for his assistance in conducting this study. We wish a Happy 100th Anniversary to Xiamen University on April 6th, 2021.

Aroyan, J. L., Cranford, T. W., Kent, J., and Norris, K. S. (**1992**). "Computer modeling of acoustic beam formation in *Delphinus delphis*," J. Acoust. Soc. Am. **92**, 2539–2545.
Aroyan, J. L. (**2001**). "Three-dimensional modeling of hearing in *Delphinus delphis*," J. Acoust. Soc. Am. **110**, 3305–3318.
Au, W. W. L., Floyd, R. W., and Haun, J. E. (**1978**). "Propagation of Atlantic bottlenose dolphin echolocation signals," J. Acoust. Soc. Am. **64**, 411–422.
Au, W. W. L., Schusterman, R. J., and Kersting, D. A. (**1980**). *Sphere-Cylinder Discrimination via Echolocation by Tursiops Truncates* (Springer, Boston), pp. 859–862.
Au, W. W. L., and Moore, P. W. B. (**1984**). "Receiving beam patterns and directivity indices of the bottlenose dolphin *Tursiops truncatus*," J. Acoust. Soc. Am. **75**, 255–262.
Au, W. W. L., and Turl, C. W. (**1991**). "Material composition discrimination of cylinders at different aspect angles by an echolocating dolphin," J. Acoust. Soc. Am. **89**, 2448–2451.
Au, W. W. L., and Pawloski, D. A. (**1992**). "Cylinder wall thickness difference discrimination by an echolocating Atlantic bottlenose dolphin," J. Comp. Physiol. A. **170**, 41–47.
Au, W. W. L. (**1993**). *The Sonar of Dolphins* (Springer, New York).
Au, W. W. L., Pawloski, J. L., Nachtigall, P. E., Blonz, M., and Gisiner, R. C. (**1995**). "Echolocation signals and transmission beam pattern of a false killer whale (*Pseudorca crassidens*)," J. Acoust. Soc. Am. **98**, 51–59.
Au, W. W. L., Kastelein, R. A., Rippe, T., and Schooneman, N. M. (**1999**). "Transmission beam pattern and echolocation signals of a harbor porpoise (*Phocoena phocoena*)," J. Acoust. Soc. Am. **106**, 3699–3705.
Au, W. W. L., Benoit-Bird, K. J., and Kastelein, R. A. (**2007**). "Modeling the detection range of fish by echolocating bottlenose dolphins and harbor porpoises," J. Acoust. Soc. Am. **121**, 3954–3962.
Au, W. W. L., Branstetter, B. K., Benoit-Bird, K. J., and Kastelein, R. A. (**2009**). "Acoustic basis for fish prey discrimination by echolocating dolphins and porpoises," J. Acoust. Soc. Am. **126**, 460–467.
Aubauer, R., Au, W. W. L., Nachtigall, P. E., Pawloski, D. A., and DeLong, C. M. (**2000**). "Classification of electronically generated phantom targets by an Atlantic bottlenose dolphin (*Tursiops truncatus*)," J. Acoust. Soc. Am. **107**, 2750–2754.

Baumann-Pickering, S., Simonis, A. E., Oleson, E. M., Baird, R. W., Roch, M. A., and Wiggins, S. M. (**2015**). "False killer whale and short-finned pilot whale acoustic identification," Endang. Species. Res. **28**, 97–108.
Brill, R. L., Sevenich, M. L., Sullivan, T. J., Sustman, J. D., and Witt, R. E. (**1988**). "Behavioral evidence for hearing through the lower jaw by an echolocating dolphin (*Tursiops truncatus*)," Mar. Mammal. Sci. **4**, 223–230.
Brill, R. L., and Harder, P. J. (**1991**). "The effects of attenuating returning echolocation signals at the lower jaw of a dolphin (*Tursiops truncatus*)," J. Acoust. Soc. Am. **89**, 2851–2857.
Bullock, T. H., Grinnell, A. D., Ikezono, E., Kameda, K., Katsuki, Y., Nomoto, M., Sato, O., Suga, N., and Yanagisaw, K. (**1968**). "Electrophysiological studies of central auditory mechanisms in cetaceans," Zeitschrift für vergleichende Physiologie **59**, 117–156.
Busnel, R. G., and Dziedzic, A. (**1967**). "Resultats Metrologiques Experimentaux de L'echolocation chez le *Phocoena phocoena* et leur Comparison avec Ceux de Certaines Chauves-souris," in Animal Sonar *System, Biology* Bionics (Laboratoire de Physiologie Acoustique, Jouy-en-Josas, France), pp. 307–335.
Cranford, T. W., Amundin, M., and Norris, K. S. (**1996**). "Functional morphology and homology in the odontocete nasal complex: Implications for sound generation," J. Morphol. **228**, 223–285.
Cranford, T. W., Krysl, P., and Hildebrand, J. A. (**2008**). "Acoustic pathways revealed: Simulated sound transmission and reception in Cuvier's beaked whale (*Ziphius cavirostris*)," Bioinsp. Biomim. **3**, 016001.
DeLong, C. M., Au, W. W. L., Lemonds, D. W., Harley, H. E., and Roitblat, H. L. (**2006**). "Acoustic features of objects matched by an echolocating bottlenose dolphin," J. Acoust. Soc. Am. **119**, 1867–1879.
Dong, J. C., Song, Z. C., Li, S., Gong, Z. N., Li, K., Zhang, P. J., Zhang, Y., and Zhang, M. (**2017**). "Acoustic properties of a short-finned pilot whale head with insight into temperature influence on tissues' sound velocity," J. Acoust. Soc. Am. **142**, 1901–1912.
Evans, W. W., and Powell, B. A. (**1967**). "Discrimination of different metallic plates by an echolocating delphinid," in *Animal Sonar Systems: Biology and Bionics*, edited by R. G. Busnel (Labaoratoire de Physiologie Acoustique, Jouy-en-Josas, France), pp. 363–382.
Feng, W., Zhang, Y., and Wei, C. (**2019**). "A biosonar model of finless porpoise (*Neophocaena phocaenoides*) for material composition discrimination of cylinders," J. Acoust. Soc. Am. **146**, 1362–1370.
Finneran, J. J., Mulsow, J., Branstetter, B., Moore, P., and Houser, D. S. (**2016**). "Nearfield and farfield measurements of dolphin echolocation beam patterns: No evidence of focusing," J. Acoust. Soc. Am. **140**, 1346–1360.
Graf, S., Megill, W. M., Blondel, P., and Clift, S. E. (**2008**). "Investigation into the possible role of dolphins' teeth in sound reception," J. Acoust. Soc. Am. **123**, 3360–3360.
Greenhow, D. R., Brodsky, M. C., Lingenfelser, R. G., and Mann, D. A. (**2014**). "Hearing threshold measurements of five stranded short-finned pilot whales (*Globicephala macrorhynchus*)," J. Acoust. Soc. Am. **135**, 531–536.
Kellogg, W. N. (**1958**). "Echo ranging in the porpoise," Science **128**, 982–988.
Li, S. H., Wang, D., Wang, K. X., Taylor, E. A., Emilie Cros, E., Shi, W. J., Wang, Z. T., Fang, L., Chen, Y. F., and Kong, F. M. (**2012**). "Evoked-potential audiogram of an Indo-Pacific humpback dolphin (*Sousa chinensis*)," J. Exp. Biol. **215**, 3055–3063.
Madsen, P. T., Kerr, I., and Payne, R. (**2004**). "Echolocation clicks of two free-ranging, oceanic delphinids with different food preferences: False killer whales *Pseudorca crassidens* and Risso's dolphins *Grampus griseus*," J. Exp. Biol. **207**, 1811–1823.
Mooney, T. A., Nachtigall, P. E., Castellote, M., Taylor, K. A., Pacini, A. F., and Esteban, J. A. (**2008**). "Hearing pathways and directional sensitivity of the beluga whale, *Delphinapterus leucas*," J. Exp. Mar. Biol. Ecol. **362**, 108–116.
Castellote, M., Mooney, T. A., Quakenbush, L., Hobbs, R., Goertz, C., and Gaglione, E. (**2014**). "Baseline hearing abilities and variability in wild beluga whales (*Delphinapterus leucas*)," J. Exp. Biol. **217**, 1682–1691.
Mooney, T. A., Yang, W. C., Yu, H. Y., Ketten, D. R., and Jen, I. F. (**2015**). "Hearing abilities and sound reception of broadband sounds in an adult Risso's dolphin (*Grampus griseus*)," J. Comp. Physiol. A. **201**, 751–761.
Mooney, T. A., Castellote, M., Quakenbush, L., Hobbs, R., Gaglione, E., and Goertz, C. (**2018**). "Variation in hearing within a wild population of beluga whales (*Delphinapterus leucas*)," J. Exp. Biol. **221**, jeb171959.
Møhl, B., Au, W. W. L., Pawloski, J., and Nachtigall, P. E. (**1999**). "Dolphin hearing: Relative sensitivity as a function of point of application of a contact sound source in the jaw and head region," J. Acoust. Soc. Am. **105**, 3421–3424.
Nachtigall, P. E. (**1980**). *Odontocete Echolocation Performance on Object Size, Shape and Material* (Springer, Boston), pp. 71–95.
Norris, K. S., Prescott, J. H., Asa-Dorian, P. V., and Perkins, P. (**1961**). "An experimental demonstration of echolocation behavior in the porpoise, *Tursiops truncatus* (Montagu)," Biol. Bull. **120**, 163–176.
Norris, K. S. (**1964**). *Some Problems of Echolocation in Cetaceans* (Pergamon, New York), pp. 316–336.
Norris, K. S. (**1968**). *The Evolution of Acoustic Mechanisms in Odontocete Cetaceans* (Yale University Press, New Haven), pp. 297–324.
Olsen, P. A. (**2009**). *Pilot Whales* (Academic, New York), pp. 847–852.
Pack, A. A., Herman, L. M., Hoffmann-Kuhnt, M., and Branstetter, B. K. (**2002**). "The object behind the echo: Dolphins (*Tursiops truncatus*) perceive object shape globally through echolocation," Behav. Proc. **58**, 1–26.
Popov, V. V., Supin, A. Y., Nechaev, D. I., Lemazina, A. A., and Sysueva, E. V. (**2019**). "Position of an acoustic window in a beluga whale: Computation based on auditory evoked potential latencies," J. Acoust. Soc. Am. **145**, 3578–3585.
Qiao, G., Qing, X., Feng, W., Liu, S., Nie, D., and Zhang, Y. (**2017**). "Elastic feature of cylindrical shells extraction in time-frequency domain using biomimetic dolphin click," J. Acoust. Soc. Am. **142**, 3787–3795.
Schevill, W. E., and Lawrence, B. (**1956**). "Food-finding by a captive porpoise (*Tursiops truncates*)," Breviora **53**, 1–15.
Song, Z. C., Xu, X., Dong, J. C., Xing, L. R., Zhang, M., Liu, X. C., and Berggren, P. (**2015**). "Acoustic property reconstruction of a pygmy sperm whale (*Kogia breviceps*) forehead based on computed tomography imaging," J. Acoust. Soc. Am. **138**, 3129–3137.
Song, Z. C., Zhang, Y., Wei, C., and Wang, X. Y. (**2016**). "Inducing rostrum interfacial waves by fluid-solid coupling in a Chinese river dolphin (*Lipotes vexillifer*)," Phys. Rev. E **93**, 012411
Song, Z. C., Zhang, Y., Mooney, T. A., Smith, A. B., and Xu, X. H. (**2018**). "Investigation on acoustic reception pathways in finless porpoise (*Neophocaena asiaorientalis sunameri*) with insight into an alternative pathway," Bioinsp. Biomim. **14**, 016004
Urick, R. J. (**1983**). *Principles of Underwater Sound*, 3rd ed. (McGraw-Hill, New York).
Wei, C., Au, W. W. L., Ketten, D. R., Song, Z. C., and Zhang, Y. (**2017**). "Biosonar signal propagation in the harbor porpoise's (*Phocoena phocoena*) head: The role of various structures in the formation of the vertical beam," J. Acoust. Soc. Am. **141**, 4179–4187.
Wisniewska, D. M., Ratcliffe, J. M., Beedholm, K., Christensen, C. B., Johnson, M., Koblitz, J. C., and Madsen, P. T. (**2015**). "Range-dependent flexibility in the acoustic field of view of echolocating porpoises (*Phocoena phocoena*)," Elife **4**, e05651.
Zhang, Y., Song, Z. C., Wang, X. Y., Cao, W. W., and Au, W. W. L. (**2017**). "Directional acoustic wave manipulation by a porpoise via multi-phase forehead structure," Phys. Rev. Appl. **8**, 064002.